Small-Scale Delay-Domain Statistics of the Frequency-Selective Indoor Wireless Channel

Wasim Q. Malik, Christopher J. Stevens and David J. Edwards
Department of Engineering Science, University of Oxford, United Kingdom
wasim.malik@eng.ox.ac.uk, david.edwards@eng.ox.ac.uk,christopher.stevens@eng.ox.ac.uk

Abstract

In this paper, electromagnetic signal propagation in the frequency-selective indoor wireless channel is investigated with the help of ultra-wideband channel measurements. Delay-domain statistics used to characterise the multipath delay spread are evaluated numerically. The spatial variation of these parameters over a short range is studied, and their statistical behaviour is analysed. It is demonstrated that the mean and rms delay spread exhibit spatially distributed alternating zones of high and low spread over a short range corresponding to electromagnetic interference fringes. Furthermore, they are approximated with Gaussian random variables. A theoretical explanation is provided for this small-scale behaviour.

1. Introduction

Propagation characterisation of wireless channels is the subject of continued research owing to the fundamental importance of channel modelling in communications system design. With the ever-growing demand for higher data rates, reliability, mobility and adaptability, the need for accurate propagation modelling is evident. In a typical narrowband system, the signal bandwidth is smaller than the channel's coherence bandwidth. As a result, flat fading is observed and time dispersion is masked by the overlapping of unresolved multipath components. In other words, as time resolution is low, multipaths arriving with small differences in their times of arrival cannot be distinguished. Such a multipath model is incapable of accurately representing the actual scattering environment, as the corresponding power delay profile does not contain precise multipath arrival information. This applies especially to dense scattering environments such as the indoor wireless channel.

In high data-rate wideband systems, the large system bandwidth permits the resolution of a large number of multipaths [1]. In this situation, accurate modelling of the multipath characteristics is even more important. Theoretical prediction of the multipath effect in such channels is sometimes performed using deterministic ray-tracing techniques, while experimental characterisation uses actual wave propagation. The delay-domain channel statistics, and especially the rms delay spread, provide sufficient information about the channel and its time-dispersion properties [2].

In this paper, the delay-domain statistics of the indoor ultra-wideband (UWB) wireless channel [3] are analysed. The parameters that can be used for complete statistical description of the channel are identified. These parameters are analysed with the help of a large set of data that was collected for this study. The small-scale variation of these delay-domain parameters is evaluated. Finally, their probabilistic distributions are estimated and the corresponding first-order statistics are calculated to characterise the multipath behaviour of the UWB indoor channel.

2. Definitions

The channel power delay profile (PDP) represents the received signal intensity as a function of excess delay [4]:

$$P_x(\tau) = \sum_{k=1}^{K} \alpha_{x,k}^2 \delta(\tau - \tau_{x,k}) \qquad (1)$$

where $_k$ is the path gain and $_k$ is the delay of the k^{th} multipath component for the spatial measurement point indexed by x. The PDP is used to derive statistical measures of the channel that are useful in channel modelling and system design. These statistics are related to the gains and delays of the multipath components resolved within the PDP. The first multipath's delay is taken to be naught, and subsequent arrivals are indexed with reference to it. The profile width is the delay $_k$ of the last multipath component K:

0-7803-8680-9/04/$20.00 ©2004 IEEE

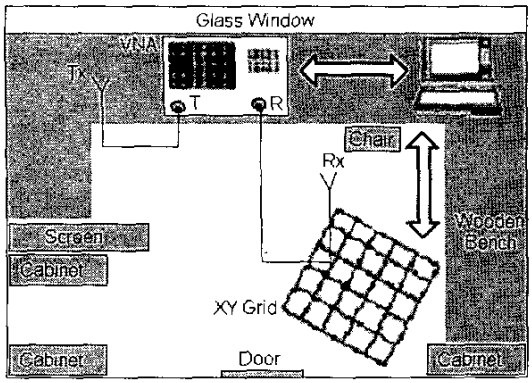

Fig. 1. Measurement setup

$$\tau_{\max} = \max(\tau_k) = (\tau_K) \tag{2}$$

The profile width provides a measure of the total duration of the multipath reverberations that correspond to a single transmitted symbol, and thus sets limits on the maximum symbol rate and channel capacity to avoid inter-symbol interference (ISI). Another useful time-domain metric is the mean delay, which is the first moment of the PDP [5], i.e.

$$\tau_{mean} = \frac{\sum_{k=1}^{K} a_k^2 \tau_k}{\sum_{k=1}^{K} a_k^2}. \tag{3}$$

The second central moment of the PDP is referred to as the rms delay spread, and is defined as

$$\tau_{rms} = \sqrt{\overline{\tau^2} - (\tau_{mean})^2}, \tag{4}$$

where '‾' denotes the expectation operator.

3. Measurement System

Complex frequency-domain channel information was collected in a typical indoor environment using a computer-interfaced vector network analyser (VNA). UWB discone antennas [6] placed at the same height were used to transmit and receive over the 4–6 GHz band with a 5 MHz spectral resolution, with a fractional bandwidth of

$$B_f = \frac{\Delta f}{f_c} = 0.4 \tag{5}$$

A computer-controlled spatial positioning system was used to gather this data in a 0.5 m x 0.5 m grid, with a 0.01 m resolution. These dimensions were selected to prevent large-scale fading while collecting sufficiently decorrelated, statistically reliable channel

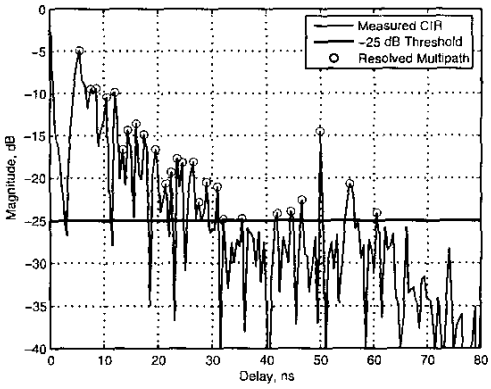

Fig. 2. A normalised indoor line-of-sight power delay profile

data. At the same time, the spatial resolution met the Nyquist criterion for the minimum wavelength in the measurement band, and provided ample resolution to study spatial variation. Since in a real indoor wireless system, it is likely for an unobstructed path to be present, this condition was replicated in the measurement. The deconvolved complex channel data $\tilde{H}_x\ f$ for each grid location x was measured. This channel data was converted to time-domain complex impulse responses $h_x\ t$ for further analysis:

$$h_x(\tau) = \sum_{k=1}^{K} \alpha_{x,k} \delta(\tau - \tau_{x,k}) e^{j\phi_{x,k}}. \tag{6}$$

where k is the time-bin index. A -25 dB noise rejection threshold was used after power-normalisation.

4. Small-Scale Spatial Variation

As a result of the experimental arrangement, the small-scale spatial variation of the delay-domain statistics can be analysed directly by observing the corresponding statistics for each individual measurement point. This variation is investigated in the current section with the help of two-dimensional diagrams that show the values of the parameter under consideration at various locations in the planar grid. In this view, the transmitter is located vertically below the bottom edge of the plot at a distance of 3.7 m. The x and y locations of grid points are indicated.

4.1. Mean Delay

The spatial variation of mean delay for the ultra-wideband indoor wireless channel is shown in Fig. 3. From inspection, its value appears to lie mostly

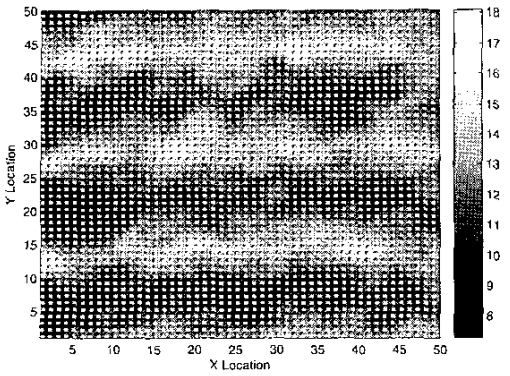

Fig. 3. Spatial variation of mean delay

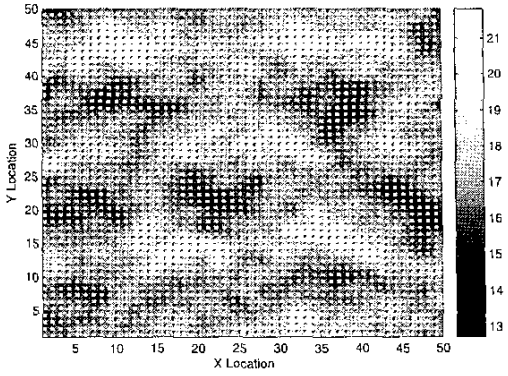

Fig. 4. Spatial variation of rms delay spread

between 10 and 15 ns, using a -25 dB PDP threshold. The plot reveals some interesting features of multipath propagation. The number of bright spots indicating high multipath spreading is comparatively higher in the top half, while receivers located near the bottom of the picture, in general, perceive lower spreads. Thus τ_{mean} increases with antenna separation. However an analysis of long-range fading behaviour is beyond the scope of the current paper. An alternating, horizontal pattern of high and low spreads can be observed. The pattern is somewhat circular, approximately aligned with the wavefronts and centred at the transmitter positioned normal to and downward from the x-axis of the plot at a distance. The wavelength of this pattern is approximately 0.15 m, which corresponds to the measurement bandwidth Δf, suggesting that a sufficient increase in Δf, as in a full-band UWB communications system, will render the fringes much more compact and thus the spreading variation practically insignificant. This is clearly an advantage of UWB technology over conventional techniques. The reason for this symmetric interference pattern is that, τ_{mean}, unlike τ_{pw}, is calculated taking into account not only multipath delays but also their gains. Thus the mean delay depends on the total received power and the Rician K-factor, both of which also display similar small-scale behaviour as revealed by our investigation. Further description of those parameters, however, is beyond the scope of the current paper.

4.2. RMS Delay Spread

It is well known that τ_{rms} is sufficient to predict the channel fading conditions, and thus has paramount importance for system design. From Fig. 4, the value of this parameter ranges mostly from 15 to 20 ns in our measurement, and is usually higher than τ_{mean}. No significant long-range correlation with distance can be observed within this area. However, nearly diamond-shaped dark "cells" are discernible, where τ_{rms} has a low value, bounded by brighter areas with higher spreads. A comparison with Fig. 1 reveals that the orientation of the interference fringes in the pattern is aligned with the walls of the room in which the propagation experiment is performed. This phenomenon relates to the physical propagation and reflection characteristics of the electromagnetic signal within the reverberation environment and indicates the presence of spatially alternating power hotspots due to multipath effect which is faithfully represented by delay spread. A comparison with Fig. 3 shows a good correlation between many of the regions where both τ_{mean} and τ_{rms} are low, such as at points (40, 35) and (5, 20) on the grid. The wavelength of the interference fringes also appears to be the same as in Fig. 3, about 0.15 m, which corresponds to Δf. The circular wave-like pattern of Fig. 3 is also replicated.

4.3. Profile Width

The respective values of the profile width τ_w over the grid are shown in Fig. 5. For a majority of the PDPs, τ_w can be observed to be between 90 and 120 ns, while its highest values approach 1.3 μs. Like τ_{mean}, there are areas with comparatively lower spreads than the surrounding points, and a good correlation is observed with Fig. 3. A comparison with Fig. 4 shows that the locations of these areas are similar to τ_{rms}.

5. Statistical Behaviour

The measurement provides channel data with

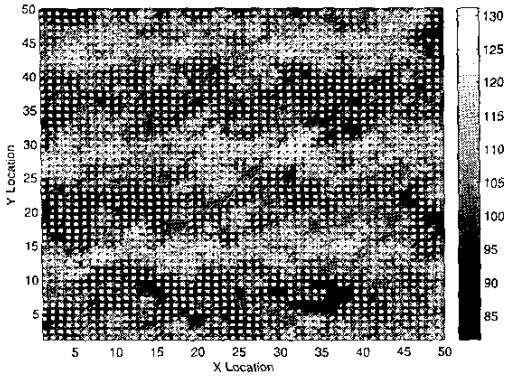

Fig. 5. Spatial variation of profile width

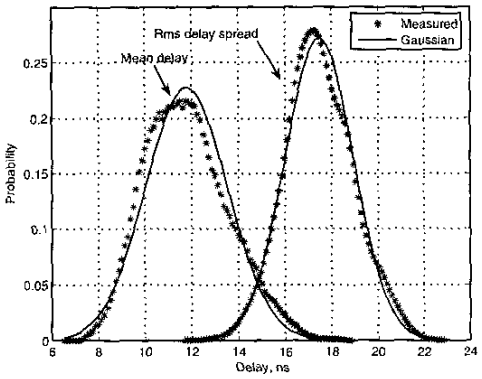

Fig. 6. Probability density estimates of τ_{mean} and τ_{rms}

sufficient generality owing to the large number of data points and their decorrelation due to multiple-wavelength coverage. This data is used to calculate the first-order statistics for τ_{rms} and τ_{mean}.

Fig. 6 shows the probability density estimates of the two quasi-continuous random variables. Both can be approximated with non-zero mean Gaussian distributions as shown. With the -25 dB threshold, the mean τ_{rms} is 17.46 ns and its standard deviation is 1.47 ns. The mean value of τ_{mean} is 11.78 ns and its standard deviation is 1.75 ns. Both are determined by the amount of multipath spreading. They are also sensitive to the noise threshold level, which corresponds to receiver sensitivity and received signal-to-noise ratio (SNR). As is intuitively obvious, if the threshold is lowered, more multipath components are included in the PDP, and the statistical descriptors are changed accordingly, increasing the spreads. Higher spreads are also expected for non-line-of-sight channels, as more mutlipaths are received while the mean multipath power and Rician K-factor are lower.

6. Discussion

The circular and rhombic patterns can be conceptually explained with the help of an optical ray-tracing model. For our measurement bandwidth, t_{res} = 0.5 ns, and therefore the spatial resolution is d_{res} = 0.15 m. Two multipath components arriving at differential delays of less than t_{res} (or path differences less than d_{res}) are perceived as a single multipath by the receiver. The two components add vectorically to yield the composite multipath component.

Consider the simple situation shown in Fig. 7, where S_1 and S_2 are two reflecting sidewalls, and the receiver assumes three successive positions on the measurement grid. The delay of the direct path P_1 arriving from the transmitter T is always shortest, followed by the two single-reflection paths P_2 and P_3 respectively, since the pathlength $T\text{-}R_k \leq T\text{-}S_1\text{-}R_k \leq T\text{-}S_2\text{-}R_k$, for $k \in \{1, 2, 3\}$.

Let us now assume that the pathlengths P_1 and P_2 are too close to be resolved by the receiver when the receiver is located at R_1, which perceives the corresponding reflections to fall within the same timebin. The reflection from P_3 however is temporally separated. The result, shown in the top graph in Fig. 8, is that the first two arrivals are merged to form a composite component with temporal blurring and magnitude alteration, while the third component is well separated. The implication is that the number of paths and their composite delays are reduced, thus reducing the delay spread. This situation corresponds to a low $_{rms}$ region, such as (40, 35) in Fig. 4.

Now if the receiver is displaced to R_2, assuming that all three paths are still incident although with varied angles of arrival, their pathlengths and thus delays are altered. If the differential delays now exceed t_{res}, all paths are cleanly resolved. The result is the middle plot in Fig. 8, which shows three distinct multipaths with their individual powers that can be modelled with an exponential decay. In this case, the delay spread is higher, such as for point (32, 30) in Fig. 4. As the receiver continues in its motion away from the transmitter and reaches point R_3 on the measurement grid, such that all three paths are still incident, it encounters a situation where P_2 and P_3 become nearly equal, thus effecting an overlap of the second and third multipaths. The number of resolved multipaths and the rms delay spread fall, as at (25, 25) in Fig. 4.

This can, at a simplistic level, be described as the movement of a given multipath component along the

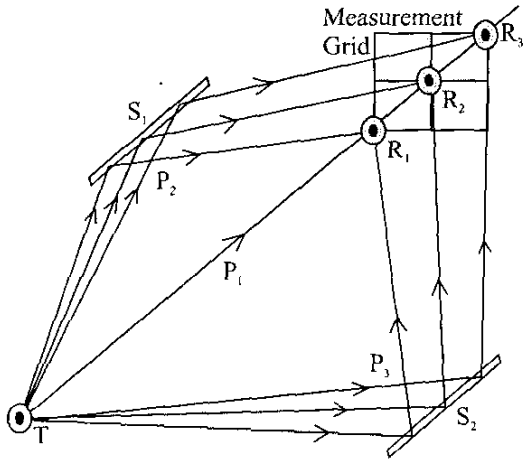

Fig. 7. Multipath propagation

delay axis, as the receiver is spatially displaced. Therefore interference fringes that reflect this behaviour can be expected, with their spatial distribution correlated with the measurement bandwidth as suggested by Fig. 3. This offers an explanation for the spatial interference pattern observed in our delay spread measurements based on the Lloyd's mirror phenomenon in optics [7].

This delay spread behaviour defines the constraints for rake combining systems [1]. The expected delay values can be used to set the initial rake finger delays. The spatial patterns provide an insight into the utility of multi-antenna techniques such as diversity and MIMO [8], and the dimensions of the interference fringes determine the optimal antenna spacing.

7. Conclusion

This study of the small-scale spatial variation in the mean delay τ_{mean}, rms delay spread τ_{rms}, and profile width τ_w provides valuable insight into the multipath propagation phenomenon in the time-dispersive ultra-wideband indoor line-of-sight channel. From our measured data, wave-like variation in τ_{mean} can be observed in the form of alternating zones of high and low values oriented along the line-of-sight (LOS) wavefronts. Diamond-shaped zones appear in τ_{rms} due to the apparent translation of a multipath component along the delay axis with receiver displacement. Similar behaviour is observed in τ_w. Gaussian random variables can be used to model τ_{mean} and τ_{rms}, with mean values of 11.78 ns and 17.46 ns respectively. The Lloyd's mirror phenomenon offers an explanation of this multipath behaviour. This delay characterisation

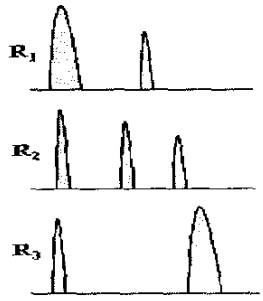

Fig. 8. Apparent multipath translation

provides valuable information for wireless channel modelling and system design. The statistical properties of the delay parameters are useful in devising channel models. The spatially varying delay properties define constraints on the design of rake, diversity and MIMO systems.

7. References

[1] W. Q. Malik, D. J. Edwards, and C. J. Stevens, "Experimental evaluation of Rake receiver performance in a line-of-sight ultra-wideband channel," in *Proc. Joint IEEE UWBST & IWUWBS*. Kyoto, Japan, 18-21 May 2004.

[2] "Propagation data and prediction methods for the planning of indoor radiocommunication systems and radio local area networks in the frequency range 900 MHz to 100 GHz," Recommendation ITU-R P.1238-3.

[3] B. Allen, T. Brown, K. Schwieger, E. Zimmermann, W. Malik, D. Edwards, L. Ouvry, and I. Oppermann, "Ultra wideband: technology and future perspectives," in *Proc. 12th WWRF*. Toronto, Canada, 4-5 November 2004.

[4] J. G. Proakis, *Digital Communications*, 4th ed. New York, USA: McGraw-Hill, 2001.

[5] G. L. Stüber, *Principles of Mobile Communications*, 2nd ed. Norwell, MA, USA: Kluwer Academic Publishers, 2001.

[6] W. Q. Malik, C. J. Stevens, and D. J. Edwards, "Spatio-spectral normalisation for ultra wideband antenna dispersion," in *Proc. 9th IEEE HFPSC*. Manchester, UK, 6-7 September 2004.

[7] E. Hecht and A. Zajac, *Optics*, 4th ed. London, UK: Addison-Wesley, 2001.

[8] W. Q. Malik, M. C. Mtumbuka, D. J. Edwards, and C. J. Stevens, "Performance analysis of ultra-wideband spatial MIMO communication systems," in *Proc. 61st IEEE VTC*. Stockholm, Sweden, 30 May 2005 (submitted).